Indian J. Phys. **70A** (1), 25–36 (1996)

IJP A
— an international journal

Simplified microscopic study of heavy-ion elastic scattering above the Coulomb barrier

Ashok Kumar

D B S (PG) College, Dehradun-248 001, India

Abstract : The study of elastic scattering provides us with basic information about the "global" properties of the heavy-ion interaction. Fully microscopic approaches like the resonating group method (RGM) and the generator coordinate method (GCM) are difficult to apply in all but the simplest of cases of the collision between two composite fragments. Hence, a simple microscopic method that accounts for the essential features of RGM and GCM in a good approximation has been used to calculate DCS for 4n heavy-ions upto 40Ca. For this purpose, the direct potential from the single channel RGM equation is used as real part of the nuclear potential and is calculated microscopically using the equivalence between RGM and GCM. Exchange effects are considered macroscopically The absorption effects due to opening of non-elastic channels are taken into account approximately in three ways, namely by sharp cut-off model, assumed and energy-dependent forms of the imaginary potential 'Anomalous large angle scattering' ALAS and "threshold anomaly" have also been discussed. The calculated results are in good agreement with the available data

Keywords : Heavy-ion elastic scattering, semi-microscopic calculations

PACS No. : 25.70.–z

1. Introduction

The general physical description of the many processes occurring in heavy-ion (HI) reaction depends on the impact parameter b. At high energies, this is related to the corresponding orbital angular momentum l by the semi-classical expression,

$$l\hbar = m\, v\, b \simeq k\, \hbar\, b. \tag{1.1}$$

Thus, one can use either b or l to characterise the type of interaction. At energies below the Coulomb barrier (E_B), the ions do not touch each other and can interact only through the Coulomb field so that Rutherford scattering results. At higher energies, the ions interact through the nuclear potential too. Then if $b \approx (R_1 + R_2)$, a grazing collision takes place, and the ions can interact elastically or inelastically or a few nucleons can be transferred from

one to the other; these may be referred to collectively as peripheral interactions. When the impact parameter is further reduced, the ions begin to interact very strongly resulting in 'strongly damped' or 'deep inelastic' collisions. Alternatively, these ions can fuse together for a short while to form compound system that decays by emission of nucleons and alpha particles.

Elastic scattering is a basic but by no means simple process in HI collisions. It is basic because it accompanies every reaction, and a thorough understanding of elastic scattering is prerequisite for a valid description of non-elastic processes. It is not simple because the complexities of many body problem implies that elastic scattering takes place in the presence of many open reaction channels, especially in the physically interesting region near and above the E_B. Thus, it would be improper to deal with elastic scattering in isolation. However, it is well known how to represent the feed back of such channels on elastic scattering by an effective interaction. Hence, construction of effective interaction must be an integral part of describing heavy-ion elastic scattering. Since a vast literature exists on the subject [1], the scope of the paper is limited to cover the essential features of the HI elastic scattering from a fundamental viewpoint.

1.1. Theoretical methods for HI collisions [2]

In the theoretical description of HI collisions, two seemingly contradictory approaches are widely used,

(i) Microscopic descriptions such as the resonating group method (RGM) or the generator coordinate method (GCM), which are based on many nucleon wave functions for the internal states of the reacting ions and effective nucleon-nucleon interactions. However, in these approaches the exact treatment of the Pauli principle leads to very complicated, highly non-local potentials.

(ii) Simple potential model description in which the dynamics of interacting nuclei is described by a Schrödinger equation with simple assumed local potential which may be derived by fitting experimental data (*e.g.* optical model, DWBA), or from some semimicroscopic or microscopically founded formalism (*e.g.* folding model).

The microscopic approach is difficult to apply in all but the simplest of cases because it encounters several difficulties owing to lack of knowledge of the nucleon-nucleon interaction and to the mathematical intractability of the many body problem. On the other hand, the purely phenomenological application of the simple potential picture invites the danger of introducing too many adjustable parameters, so that available data are reproduced but the predictive power of the model is lost.

It is most important to realize that fully microscopic models along the lines of the RGM or GCM and simple potentials models do not contradict each other. In fact, rewriting the equations of motion of the RGM or GCM in the form of collective Schrödinger equation establishes a quantitative relation between effective interaction potentials and microscopic matrix elements of the many-nucleon Hamiltonian, and this relation can be used to derive

or justify the input of the simple potential models. Such a derivation of simple (local) nucleus-nucleus potentials from microscopically calculated matrix elements of the many-nucleon Hamiltonian, was first discussed by Friedrich and Canto in 1977 and has since been applied with remarkable success to the elastic scattering of a wide range of open and closed shell nuclei. Recently Horiuchi and collaborators have also developed methods to derive local nucleus-nucleus potentials from the non-local integral kernels of the RGM. However, these methods do not calculate the DCS explicitly and other peculiar features of elastic scattering are also not described.

Hence, the central theme of the present article is to develop simplified microscopic description of elastic scattering which contains essential features of both RGM and GCM avoiding, however, their complexities. For this purpose, in section 2, the direct potential from the single channel RGM equation is used as real part of the nuclear potential and is calculated microscopically using the equivalence between RGM and GCM [3]. Exchange effects are considered macroscopically [4]. The absorption effects are taken into account approximately. "Anomalous Large Angle Scattering" (ALAS) and 'threshold anomaly' phenomena are also discussed. In section 3, some specific examples are discussed which allow a direct comparison of calculated DCS with experimental ones.

2. Formulation

As starting point, rewrite time-independent Schrödinger equation.

$$(H - Et)\,\Psi = 0 \tag{2.1}$$

In RGM and GCM good approximate solution of the related many body Schrödinger equation is obtained by writing it in the form of a variational or projection equation [5]

$$\langle \delta\Psi \,|\, H - Et |\, \Psi \rangle = 0 \tag{2.2}$$

where, E_t is the total energy of the system, and restricting Ψ to a limited region of the Hilbert space of the translational invariant Hamiltonian operator H. The N-nucleon Hamiltonian is taken as

$$H = \sum_{i=1}^{N} - \frac{\hbar^2}{2M} \nabla_i^2 + \sum_{i<j=1} V_{ij} - T_{cm} \tag{2.3}$$

where, N is the number of nucleons, T_{cm} is the kinetic energy operator of the center-of-mass of the total system, and V_{ij} is the nucleon-nucleon potential. The main advantage of this procedure is that the trial wave function can be made so flexible that from the very beginning one can introduce jointly the boundary conditions. This flexibility is needed since the properties of nuclei vary considerably form nucleus to necleus and even from level to level.

Both RGM and GCM employ (2.2) with different general forms for the trial wave function Ψ. The RGM leads to the conversion of eq. (2.2) into integro differential equations to be solved for the relative motion functions while GCM leads to integral

equations to be solved for the weight functions. These two methods were developed independently but are closely related to each other.

In the present investigation, one can start with RGM and the equivalence between RGM and GCM will be exploited later in the microscopic calculation of real part of nuclear potential. In the single-channel RGM, consider scattering of nuclei numbered 1 and 2. Now trial wave function Ψ is called Ψ_R as

$$\Psi_R = A\,\Phi_1\Phi_2\,F\left(\boldsymbol{R}_1, \boldsymbol{R}_2\right)\Omega\,(\sigma,\tau) \tag{2.4}$$

where Ω is the spin-isospin function for the system, A is the antisymmetrization operator, Φ_1 and Φ_2 are the two wave function for the clusters 1 and 2. F describes the relative motion of the two clusters and is a function of the distance between their centers-of-mass $\boldsymbol{R}_1$ and $\boldsymbol{R}_2$. For the solution of eq. (2.2) the set of basis functions in the limited Hilbert space are found by writing the wave function eq. (2.4) in the following form using the delta function,

$$\Psi_R = A\left[\int \Phi_1\,\Phi_2\,F\,(\boldsymbol{R}')\,\delta\,(\boldsymbol{R}' - \boldsymbol{R})\,d\boldsymbol{R}'\right] \tag{2.5}$$

In eq. (2.5), the spin-isospin part has been included in the cluster functions Φ_1 and Φ_2 and $\boldsymbol{R} = \boldsymbol{R}_1 - \boldsymbol{R}_2$.

Eq. (2.2) now becomes,

$$\left\langle A\left[\Phi_1\,\Phi_2\,\delta\,(\boldsymbol{R}' - \boldsymbol{R})\right]\left|H - E_t\right|A\left[\Phi_1\,\Phi_2\,F(\boldsymbol{R}')\right]\right\rangle = 0 \tag{2.6}$$

where the brackets imply integration over the internal co-ordinate x_1 and x_2 of the clusters and $\boldsymbol{R}'$ but not on $\boldsymbol{R}$. Eq. (2.6) reduces to,

$$\left\langle\left[\Phi_1\,(\xi_1)\,\Phi_2\,(\xi_2)\right]\left|H - E_t\right|A\left[\Phi_1\,(\xi_1)\,\Phi_2\,(\xi_2)\,F(\boldsymbol{R})\right]\right\rangle = 0 \tag{2.7}$$

The operator A is decomposed as $A = \hat{A}\,A_1\,A_2$ and eq. (2.7) becomes

$$\begin{aligned}&<\left[(A_1\Phi_1(\xi_1))\,(A_2\Phi_2(\xi_2))\right]\left|H - E_t\right|\hat{A}\\ &\qquad\left[(A_1\Phi_1(\xi_1))\,(A_2\Phi_2(\xi_2))\,F(\boldsymbol{R})\right] > = 0\end{aligned} \tag{2.8}$$

where, A_1 is the antisymmetization operator w.r.t. the nucleons of nucleus 1. A_2 is w.r.t. nucleons of nucleus 2 and $\hat{A}$ is the rest antisymmetrizer *i.e.* for the remaining permutations of the nucleons between nuclei 1 and 2. Writing $\hat{A}$ as $1 + (\hat{A} - 1)$, one may finally get a simplified form of RGM,

$$\left[-\frac{\hbar^2}{2\mu}\nabla_R^2 - E + V_D(R)\right]F(\boldsymbol{R}) + \int K(\boldsymbol{R},\boldsymbol{R}')\,F(\boldsymbol{R}')\,d\boldsymbol{R}' = 0 \tag{2.9}$$

where, E ($= E_t - E_1 - E_2$) is energy of the relative motion, $V_D(R)$ is a local or direct potential and $K(\boldsymbol{R},\boldsymbol{R}')$ are the non-local kernels. The $V_D(R)$ may be taken as the sum of

real nuclear potential $V_R(R)$ and the coulomb part $V_C(R)$. Since, non-local kernels representing the exchange effects are very difficult to be evaluated for Heavy-ions, a macroscopic approach is adopted here by replacing the non-local kernels with a local potential $V_{ex}(R)$ of shorter range than $V_R(R)$. Eq. (2.9) reduces to differential form and to solve it, the familiar partial wave expansion of $F(\boldsymbol{R})$ is used.

$$\frac{d^2 f_l(R)}{dR^2} + \left[k^2 - \frac{2\mu}{\hbar^2}\left\{\frac{l(l+1)\hbar^2}{2\mu R^2} + V_c(R) + V_R(R) + V_{ex}(R)\right\}\right] \times f_l(R) = 0 \tag{2.10}$$

where μ is the reduced mass and

$$V_{ex}(R) = c \exp\left[-\lambda_e R^2\right] V_R(R) \tag{2.11}$$

The two parameters c and λ_e are to be adjusted to get best fit with data. Caution must be observed to select these values which should give finite magnitude of $V_{ex}(R)$ in the tail region of $V_R(R)$. $V_C(R)$ is the familiar Coulomb potential. $V_R(R)$ is given by

$$V_R(R) = \left\langle \Phi_1(\xi_1)\, \Phi_2(\xi_2) \left| \sum_{i\epsilon 1,\, j\epsilon 2} V_{ij} \right| \Phi_1(\xi_1)\, \Phi_2(\xi_2) \right\rangle R \tag{2.12}$$

Eq. (2.12) is solved using the equivalence relations between the RGM and the GCM [3].

2.1. Absorption effects

Since exact calculation of absorption effects is not possible, three approximate methods are deployed here in the following manner.

(i) Sharp cut-off approximation is an extreme assumption implying that the elastic scattering matrix rises from $|\, g_l \,| = 0$ (complete absorption) to $|\, g_l \,| = 1$ (no absorption) at a single critical value $l = l_c$ [5]

(ii) The nuclear potential is taken to be complex as

$$V_N(R) = \lambda_R V_R(R) + i\lambda_I V_I(R) \tag{2.13}$$

where, λ_R and λ_I are the adjustable parameters of real and imaginary parts of the nuclear potential. Following Canto (6) eq. (2.13) becomes ($\lambda_R = 1$ and $\lambda_I = \lambda$)

$$V_N(R) = V_R(R) + i\lambda V_R(R) \tag{2.14}$$

(iii) Since the absorption effects are energy dependent, the following energy-dependent form of the imaginary potential would be more appropriate (7).

$$V_I(R) = W(\lambda, E) f(R) \tag{2.15}$$

with $$W(\lambda, E) = \frac{\hbar^2}{2\mu}\lambda\left\{\frac{\lambda^2}{4}+\frac{2\mu}{\hbar^2}\left[E_{cm}-V_R(R)\right]\right\}^{\frac{1}{2}} \tag{2.16}$$

where, λ is the adjustable parameter, E_{cm} is the center-of-mass energy and μ the reduced mass. $f(R)$ is a smooth exponetial function given by,

$$f(R) = \frac{\exp\left[-\frac{R}{2}\right]}{R} \tag{2.17}$$

Applying one of the methods for absorption effects, eq. (2.10) is numerically solved for each $f(R)$ value and then nuclear phase shifts are computed by using 'RCWFN Program' [5] for the regular and irregular Coulomb wave functions. The required Coulomb phase shift are also easily computed by familiar technique, knowing nuclear and coulomb phase shifts, scattering amplitude $f(\theta)$ can be calculated from the partial wave expansion using the Legender polynomials. Finally, DCS ($\sigma(\theta)$) are obtained from the relation,

$$\sigma(\theta) = |f(\theta)|^2$$

2.2. Anomalous Large Angle Scattering (ALAS)

It has been demonstrated in many heavy-ion scattering experiments that large rising and oscillating cross sections are present at large angles. Since these cross sections often exceed the Rutherford value, the scattering phenomenon has been termed 'anomalous'. It is observed noticeably in α particle scattering but also with various heavy-ions.

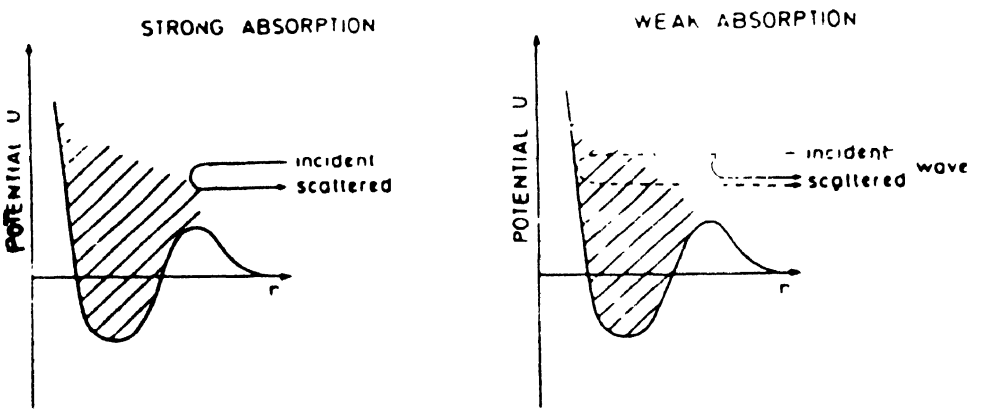

Figure 1. Schematic representation of strong and weak absorption in an interaction potential of colliding nuclei.

Since, conventional optical potential fails to explain 'ALAS', a variety of theoretical interpretations, based on dynamical models or on purely phenomenological assumptions, have been proposed to explain or merely reproduce these features. A list of such proposals includes Regge poles, shape resonances, quasimolecular resonances, continuum rotational

bands with variable moments of inertia, barrier top resonances, elastic transfer *etc.* There is as yet no satisfactory physical explanation. Hence, it is worthwhile to seek its explanation within our framework. It has been shown that a potential model description of ALAS requires both relatively weak absorption and a real potential deep enough to provide a "classical pocket" inside the Coulomb barrier [8].

It is evident from Figure 1 that when absorption is strong, the internal wave is damped and the outer barrier wave leads to a normal diffraction pattern. However, when absorption is weak, the influence of the internal wave becomes stronger and DCS display ALAS.

2.3. Threshold anomaly [9]

The main features of 'threshold anomaly' are that the strength of the imaginary potential, in the surface region to which the elastic scattering is sensitive, increases rapidly as the energy rises above the coulomb barrier and then saturates while at the same time the real, attractive potential in the same region decreases rapidly and then remains more or less constant. The behaviour of the absorption potential $W(E)$ is easy to understand because the Coulomb barrier closes the non elastic channels at the lower energies but increasing the energy above the barrier allows absorption to take place. Hence, the word "threshold". The term 'anomaly' applies to the real potential $V_R(E)$ whose behaviour was unexpected. Figure 2 shows the canonical example. It has been confirmed that the above behaviour is a coupled channels

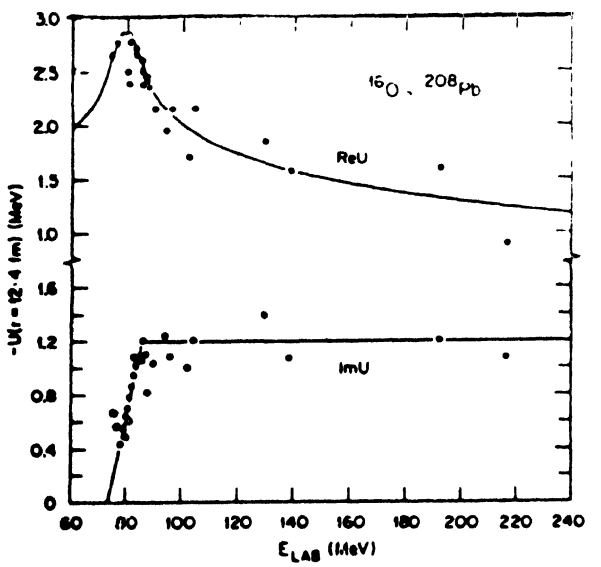

Figure 2. Optical potential strengths for $^{16}O + ^{208}Pb$ system.

(CC) effect. Effective real potential correction ("polarization potentials") have been extracted from these calculations and agree with the "anomaly". Such CC calculations are complicated and specific to each system. However, a more general approach includes all the

CC dispersive effects "exactly" by using a dispersion relation between $V_R(E)$ and $W(E)$. This ensures that if the absorption varies, there will be a corresponding anomaly in the real potential near E_B. Thus, it should be a universal phenomenon. However, obtaining similar data for other heavy-ions remain an experimental challenge because of resolution problem to separate the elastic and inelastic events. Another difficulty is the dominance of the Coulomb interaction for bombarding energies close to E_B resulting Rutherford scattering and so do not contain much information about 'threshold anomaly'.

3. Results and discussion

The simplified microscopic approach discussed in section 2 is applied to study the elastic scattering of different 4n-HI systems upto ^{40}Ca. Results of some of the specific and interesting cases are discussed along with their strong and weak points.

3.1. Local exchange potential for $^{32}S + ^{40}Ca$ system [10]

Elastic scattering data of ^{32}S + ^{40}Ca above the E_B have been analysed using local exchange potential V_{ex} and assumed form of the imaginary potential. Four parameters are adjusted. It is found that the agreement between calculations and data improves but not significantly. Since V_{ex} does not contribute significantly in reproduction of scattering data, it will not be considered in RGM differential equation in the latter cases, thus reducing adjustment of four parameters to only two.

3.2. Characteristic features of elastic scattering of identical nuclei [11]

The elastic scattering of two identical nuclei ^{40}Ca + ^{40} Ca at various energies is discussed. One direct consequence of indistinguishability of projectile and target is that DCS is symmetrical about $\theta = \frac{\pi}{2}$. Another important consequence is the appearance of interference between two unsymmetrical amplitude $f(\theta)$ and $f(\pi - \theta)$. This is most strikingly displaced at low energies where the scattering is primarily due to Coulomb field. And one obtains

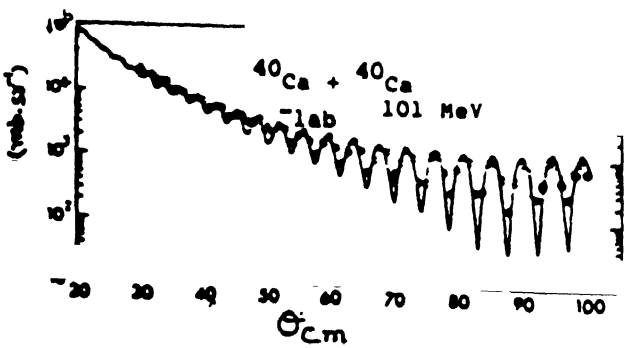

Figure 3. Optical model calculation for ^{40}Ca + ^{40}Ca elastic scattering at E_{lab} = 101 MeV is shown by solid line curve along with experimental data shown by solid circles

highly oscillatory Mott cross sections instead of the monotonic Rutherford cross sections as evident in Figure 3. As the bombarding energy is increased above E_B, absorption increases

which damps out Mott oscillations. This occurs because the Rutherford amplitude is dominated by Fresnel-like amplitude. It suggests that interference effect is greatly reduced.

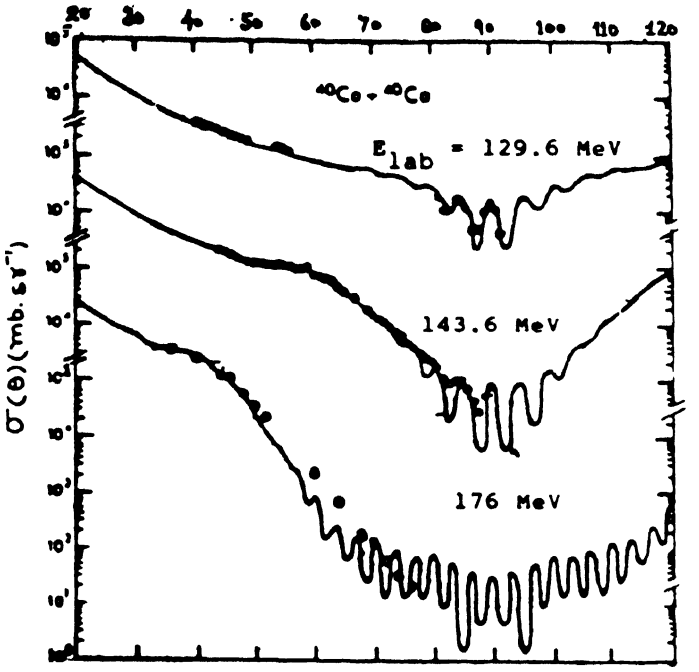

Figure 4. The calculated DCS ($\sigma(\theta)$) for ^{40}Ca + ^{40}Ca elastic scattering at E_{lab} = 129.6, 143.6 and 176 MeV are shown by solid line curves along with experimental data shown by solid circles

This has been confirmed both theoretically and experimentally as evident from the damped oscillatory pattern of the DCS at higher energies in Figure 4, where full-line curves represent the present calculations.

3.3. Evidence of heavy-Ion resonances [12]

For many years, observation of resonances was restricted to the scattering and reactions of *p*-shell nuclei. This belief was shaken by the observation of a strong backward rise in the elastic scattering of ^{28}Si + ^{28}Si at E_{lab} = 120 MeV. This is in contrast to the finding for the system ^{28}Si + ^{30}Si at a similar energy. The simplified microscopic approach using sharp cut-off model for absorption could explain the data at other lower energies [13] but failed at 120 MeV as shown in Figure 5 by top dash curve. The bottom dash-curve is the result of an optical model calculation. Since both the calculations show poor agreement, the sharp cut-off approach is replaced by second form of imaginary potential adjusted for weak absorption in the present work, in order that the standing wave resonances formed in the real potential for grazing partial waves do not become too broad. This type of calculation is shown by full-line curve which is in close agreement with data. This finding is also supported by latest ORNL, (USA), 1991 report.

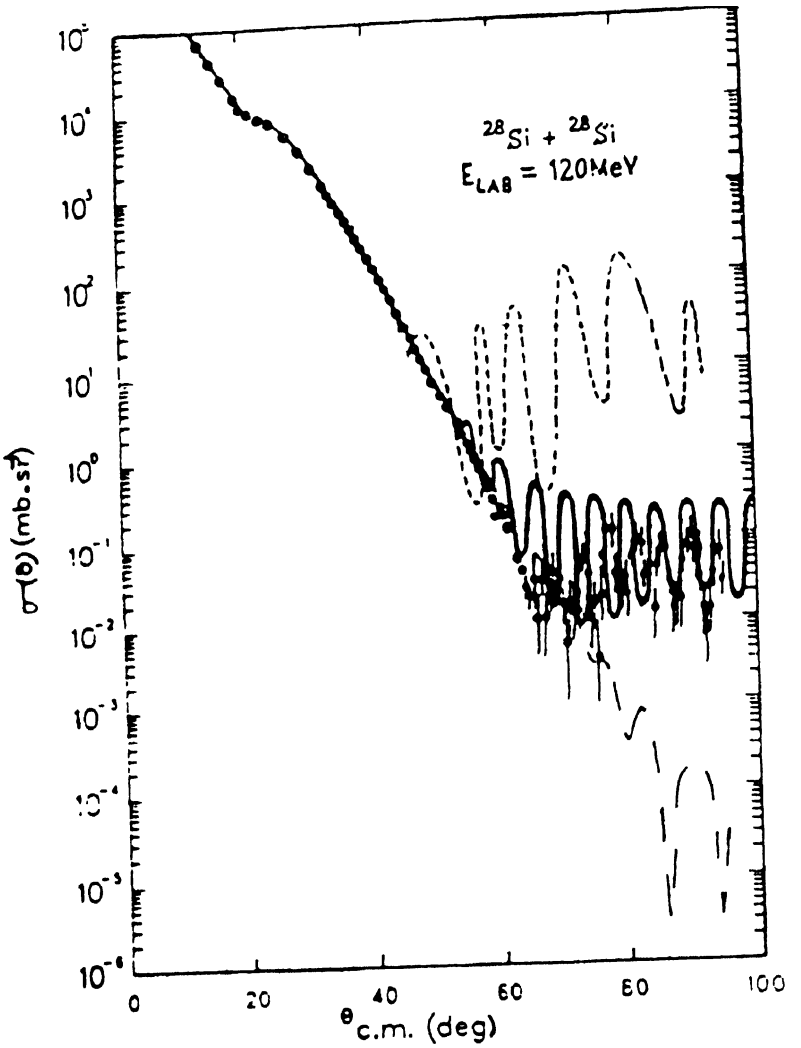

Figure 5. The calculated DCS ($\sigma(\theta)$) for $^{28}Si + ^{28}Si$ elastic scattering at E_{lab} = 120 MeV are shown by upper dotted curve for sharp cut-off, lower dash curve for optical model and middle full line curve for complex potential with weak absorption along with experimental data by solid circles

3.4. $^{32}S + ^{32}S$ elastic scattering at E_{lab} = 120 MeV using energy dependent imaginary potential

The open-shell nature of ^{32}S has made the calculations rather impractical. To avoid this we apply natural dynamical generalization of the filling approximation by considering 3/5 magnitude of the unfilled 1*d* shell thus resulting in a spherically symmetric configuration for ^{32}S. In Figure 6, DCS are first calculated with assumed form (dotted curve) [14] and then with energy-dependent form of imaginary potential (full-line curve) agreement is satisfactory in both the cases but the latter needs refinements.

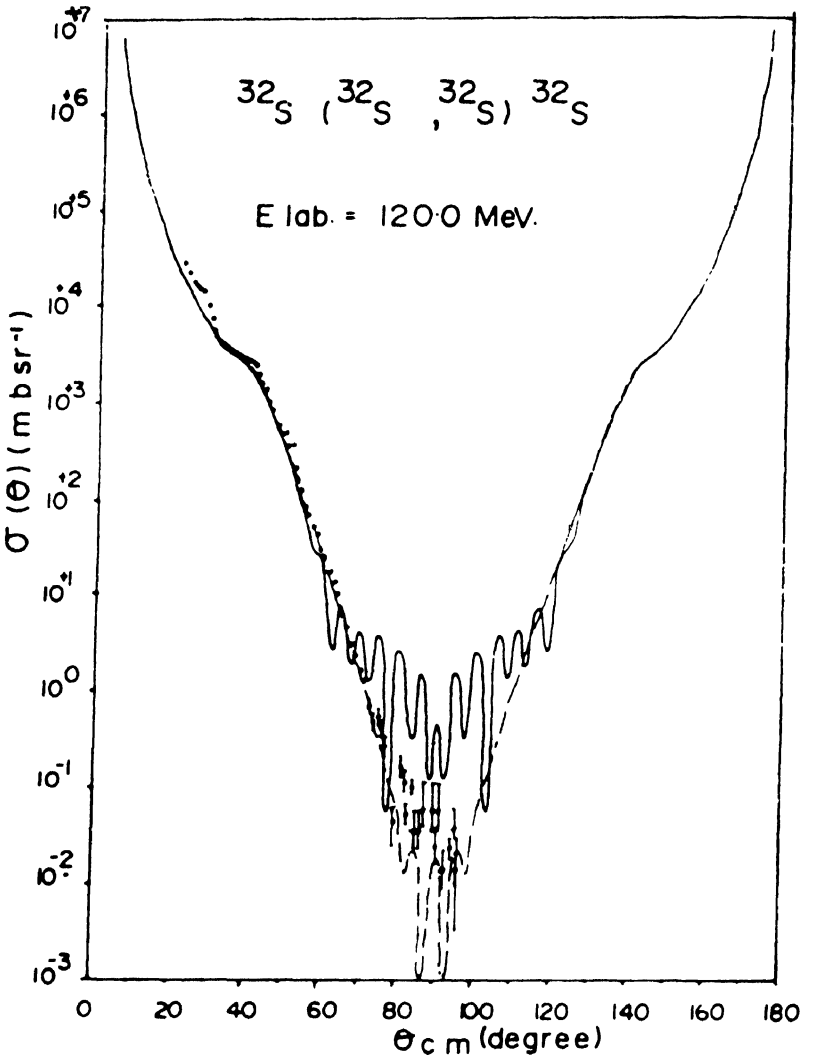

Figure 6. The calculated DCS ($\sigma(\theta)$) for $^{32}S + ^{32}S$ elastic scattering at E_{lab} = 120 MeV are shown by two curves, full line for energy-dependent and dotted line for energy-independent imaginary potential along with the experimental data with solid circles

3.5. Anomalous large angle scattering (ALAS) of $^{16}O + ^{28}Si$ at E_{lab} = 50 and 55 MeV [8]

Conventional potentials of Wood-Saxon shape fail to explain ALAS, its explanation is sought outside the domain of standard optical model. The present theory is applied for this purpose with imaginary potential adjusted for low absorption. The DCS ratio are reproduced reasonably good suggesting that ALAS is due to a conjoint effect of strong folding real potential and low absorption potential. ALAS is also investigated for ^{24}Mg (^{16}O, ^{16}O) ^{24}Mg at E_{cm} = 27.8 MeV and reported [15].

3.6. Evidence of threshold anomaly in $^{32}S + ^{40}Ca$

As pointed out in section 3.1, that $^{32}S + ^{40}Ca$ elastic scattering results are not reproduced satisfactorily near E_B suggesting the induction of polarization potential which, infact, is needed to understand threshold anomaly. A careful investigation later revealed that the strength of the imaginary potential decreases rapidly as one approaches E_B while the normalization factor for real folded nuclear potential increases abruptly and exceeds 1 in the vicinity of E_B. This is in conformity with the experimental findings of polarization potential [9] Although there are recently many, mostly qualitative, examples of this anomaly for elastic scattering, precise study to establish its characteristics is yet to come.

Hence, the simplified microscopic approach, which is not "microscopically pure" but "physically accurate" has provided a coherent account of HI elastic scattering.

References

[1] R Book *Heavy-ion Collisions* (Amsterdam North Holland) **Vol I, II, III** *and references there in* (1979, 80, 82)

[2] K Langanke and H Friedrich *Advances in Nuclear Physics* (New York Plenum) **Vol 17** Ch 2 (1986)

[3] M Kamimura and T Matsuse *Prog Theor Phys* **51** 438 (1974)

[4] Y C Tang, M LeMere and D R Thompson *Phys Rep* **47** 167 (1978)

[5] Ashok Kumar *PhD Thesis* (University of Meerut, India) (1983)

[6] L F Canto *Nucl Phys* **A 279** 97 (1979)

[7] B Fink and C Toepfler *Phys Lett* **45B** 411 (1973)

[8] Ashok Kumar, K Eswaraiah, R D Godiyal and B B Srivastava *Int Conf on Nucl Reaction Mechanism* (Calcutta, India) 6 (1989)

[9] G R Satchler *Phys Rep* **199(3)** 147 (1991)

[10] Ashok Kumar, K Eswaraiah, R D Godiyal, M Seth and B B Srivastava *4th Int Conf on Nucleus-Nucleus Collisions* (Kanazawa, Japan) 154 (1991)

[11] Ashok Kumar, R D Godiyal, K Eswaraiah and P K Bhatnagar *DAE Symp on Nucl Phys* (India) **33B** 187 (1990)

[12] R D Godiyal, Ashok Kumar, K Eswaraiah and B B Srivastava *DAE Symp on Nucl Phys* (India) **32B** 060 (1989)

[13] Ashok Kumar and B B Srivastava *Can J Phys* **66** 813 (1988)

[14] Ashok Kumar, K Eswaraiah, R D Godiyal, P K Bhatnagar and B B Srivastava *DAE Symposium on Nucl Phys* (India) **33B** 189 (1990)

[15] Ashok Kumar, R D Godiyal, Sunita Kumar and Vidula Dixit *Int Nucl Phys. Conf* (Wiesbaden, Germany) (1992)